

cRPA calculation of on-site and nearest neighbor Coulomb interaction of LaNiO_2

Long Zhang¹ and Hai-Ping Cheng¹

¹ Department of Physics and The Quantum Theory Project, University of Florida, Gainesville FL 32611, USA

We present first-principle calculation of the on-site and nearest neighbor Coulomb interaction strength of the Ni d orbitals in bulk LaNiO_2 , using the constrained Random Phase Approximation method. The nearest neighbor correlation within Ni-O plane turns out to be more significant when considering the frequency dependent $U(\omega)$, which can be as strong as about 25% of the on-site value at medium and high frequencies. The inter Ni-O plane nearest neighbor correlation is found to be the same strength as that within the Ni-O plane, indicating the material is non-locally correlated also between the Ni-O planes.

I. INTRODUCTION

Since the discovery of high-temperature superconductivity in the cuprates¹, tremendous theoretical and experimental efforts have been devoted to the physics of this family of materials²⁻⁶. Searching for the cuprate-like superconductivity candidates in the family of transition metal oxides is one of the research directions in this area. By studying the similarities and differences, theorists hope to understand the mechanism and expand the utility of superconductivity⁷ in functional materials. Although a complete and unambiguous understanding of its nature has not been reached, some essential features for superconductivity have been highlighted for searching for cuprate-like materials. The main common features include the two-dimensional electronic structure and magnetism⁴, antiferromagnetically interacting $S=1/2$ moments, substantial d-p hybridization, and the large orbital polarization (one-band physics). Nickelates have been studied along this line as a candidate of non-Cu-based but cuprate-like superconductor⁸⁻¹³. One important milestone in this direction is the discovery of superconductivity at 9-15K in the infinite-layer nickelate $\text{Nd}_{1-x}\text{Sr}_x\text{NiO}_2$ grown on SrTiO_3 substrate¹⁴⁻¹⁶. The mother compound is NdNiO_2 which was synthesized about two decades ago¹⁷ and the closely related compound LaNiO_2 was synthesized much earlier¹⁸. Early theoretical studies¹⁹ had excluded LaNiO_2 from the cuprate analogs because the d-p hybridization is weak and the Fermi surface is non-cuprate like, while recent discover of $\text{Nd}_{1-x}\text{Sr}_x\text{NiO}_2$ brought the properties of both NdNiO_2 and LaNiO_2 back to attention²⁰.

NdNiO_2 and LaNiO_2 are isostructural to the infinite-layer cuprates with a flat NiO_2 plane of the square lattice of monovalent Ni^{1+} cations. The Ni^{1+} cation has one hole in the $d_{x^2-y^2}$ orbital and possesses the same $3d^9$ electron configuration counting as Cu^{2+} cations in the undoped cuprates. Superconductivity in bulk NdNiO_2 has not been observed²¹. Pristine NdNiO_2 and LaNiO_2 have metallic behavior with no sign of long-range magnetic order down to low temperatures^{17,21,22}, suggesting a weak or mediate correlation effect. It has been pointed out that the effect of Sr doping gives a more pure single $d_{x^2-y^2}$ band cuprate-like picture²³, which makes the value of the Coulomb interaction strength of the $d_{x^2-y^2}$ orbital an important quantity to characterize the system. Indeed the on-site Coulomb interaction U was included in all theoretical and first-principle studies, and the value of on-site U are mostly empirical in the range of 3-8 eV. A dedicated calculation of U from first principle is desirable for not only the on-site cor-

relation but also the possible non-local correlation. It was pointed out that²⁴ the nearest neighbor Coulomb interaction in cuprates affects the stability of superconductivity and the phase competition among various phases. While dedicated studies on both on-site and nearest neighbor Coulomb interactions are still missing for the newly discovered Nickelate materials. We are thus motivated to calculate the on-site and the various nearest neighbor Coulomb interactions from first principle for LaNiO_2 .

Previous study²⁵ had shown that LaNiO_2 and NdNiO_2 give essentially the same band structure except for the Nd-4*f* bands. And, studying LaNiO_2 instead of NdNiO_2 helps to avoid the issue of Nd-4*f*²⁶. Therefore we study LaNiO_2 and suggest the calculated Coulomb interaction of Ni sites would be close to that of Ni in NdNiO_2 , because neither Nd *f*-like bands nor La *f*-like bands are close to the Fermi level in DFT studies of these two materials and the method we used only considers the *d*-like bands of Ni.

In the current work, we consider the following Coulomb interactions in LaNiO_2 , within Ni-O plane: the on-site $U^{o.s.}$, the nearest neighbor $U^{n.n.}$, the nearest neighbor in diagonal $U^{n.n.diag}$, the next nearest neighbor $U^{n.n.n.}$, and between two Ni in adjacent Ni-O planes: $U_{\perp}^{n.n.}$. These have been shown in Fig.1.

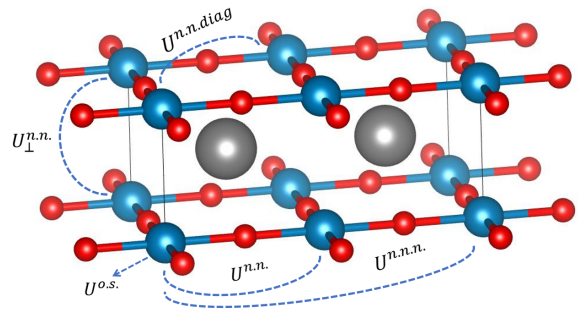


FIG. 1: Crystal LaNiO_2 is displayed in a $2 \times 1 \times 1$ supercell setup, in order to identify the various in-plane Coulomb interaction between the Ni atoms (blue balls): on-site (o.s.), nearest neighbor (n.n.), nearest neighbor in diagonal (n.n.diag) and next nearest neighbor (n.n.n.). The inter-plane nearest neighbor interaction is tagged with subscript " \perp ". Red balls are Oxygen atoms. Gray balls are Lanthanum atoms.

Outline : The remainder of the paper is organized as fol-

lows. Section II introduces the calculation methods, including the DFT and DFT results which is the base for the following constrained RPA (cRPA) calculation of the Coulomb interaction U . Section III has the resulting U matrices and the frequency dependence of several key matrix elements. Section IV provides summary and conclusion.

II. CALCULATION METHODS

In this section we first present the DFT band structure of LaNiO_2 and the orbital characters of the bands close to Fermi level that motivated the selection of the correlation window for subsequent model construction and cRPA calculation. Then we briefly go over the theory of cRPA. The resulting $U(\omega)$ is presented in the next section.

II.A. DFT calculation

The DFT calculation is done using the FP-LAPW method, as implemented in a modified version of the ELK code²⁷. The ground state is calculated within the local density approximation (LDA). The muffin tin sphere radii are $2.2 a_0$, $2.0 a_0$ and $1.6 a_0$ for La, Ni and O, respectively. A dense k-point grid of $16 \times 16 \times 16$ was used to perform Brillouin zone integration. The used lattice parameters for LaNiO_2 are $a = b = 3.96 \text{ \AA}$ and $c = 3.37 \text{ \AA}$. NdNiO_2 has slightly different lattice parameters, $a = b = 3.92 \text{ \AA}$ and $c = 3.28 \text{ \AA}$. As pointed out in²³, we also found that a non-magnetic calculation of LaNiO_2 at the lattice parameters of NdNiO_2 does not give rise to any important changes in the band structure. Thus we stick to the original LaNiO_2 lattice parameter in all calculations.

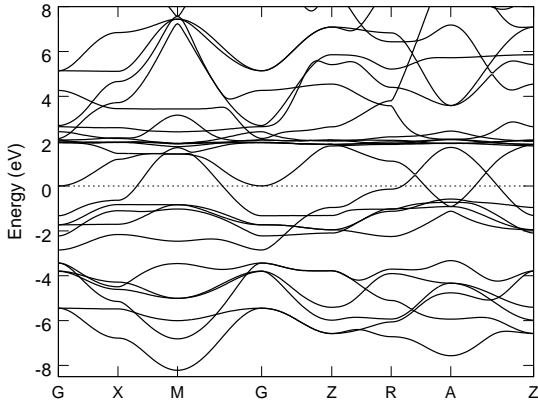


FIG. 2: Non-magnetic ground state band structure of LaNiO_2 . Fermi level is at zero.

The non-magnetic ground state band structure is shown in Fig.2. There are five d -like bands around the Fermi level in $[-3.0, +2.0] \text{ eV}$, representing the partially filled d states of Ni,

giving the material a metallic ground state. Below them in the $[-8.0, -3.0] \text{ eV}$ range are six bands showing Oxygen p orbital character. The Ni d -like bands and p -like bands are separated by a small gap. Above the Ni d -like bands, crowded at about $+2.0 \text{ eV}$, there are several flat bands of the La f character. The La d -like bands are entangled with other bands above the Fermi level with most weights about $+2.0 \text{ eV}$.

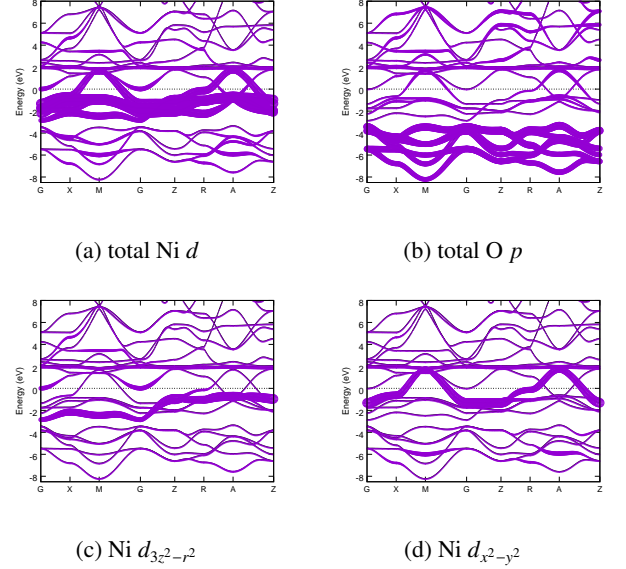


FIG. 3: Fat bands showing the amount of overlapping between Bloch states and Ni d states and O p states. (a) and (b): total d and total p character. (c) and (d): individual $d_{3z^2-r^2}$ and $d_{x^2-y^2}$ character.

The orbital character of the Bloch bands are often indicated by its overlapping with crystal field split states like the t_{2g} and e_g of the d orbital for example. That helps with identifying proper energy windows for Wannier downfolding in the next step. The Ni d -like bands and O p -like bands are identified in the fat band plots in Fig.3. It's clearly seen the Ni d weights are in $[-3.0, +2.0] \text{ eV}$ and the d - p mixing is not significant though the p weights spread up to above the f -like bands of La. The individual Ni $d_{x^2-y^2}$ character dominates around the Fermi level and is mainly responsible for the physics properties. The Ni $d_{3z^2-r^2}$ -like band is entangled with the Ni $d_{x^2-y^2}$ band in the k -path Z-R, which motivates a two-band model construction later.

The La d -like and f -like bands are separately displayed in Fig.4. From Fig.4 (a) and (b) we see the majority of La d -like bands are located above the f -like bands at $+2 \text{ eV}$ above the Fermi level. The break up of La $d_{3z^2-r^2}$ and $d_{x^2-y^2}$ in (c) and (d) help to clarify that the single band touching Fermi level from above at the Γ point is clearly not of $d_{x^2-y^2}$ character. That band actually has limited La $d_{3z^2-r^2}$ character that is bound to Γ point only, and its $d_{3z^2-r^2}$ character is not more significant than the amount of the mixing of Ni d and O p as shown in (a) and (b) in Fig.3. Based on these observations we are not encouraged to include La $d_{3z^2-r^2}$ or La $d_{x^2-y^2}$ bands in the correlation window for model construction, though it had been

done in other analysis²⁵.

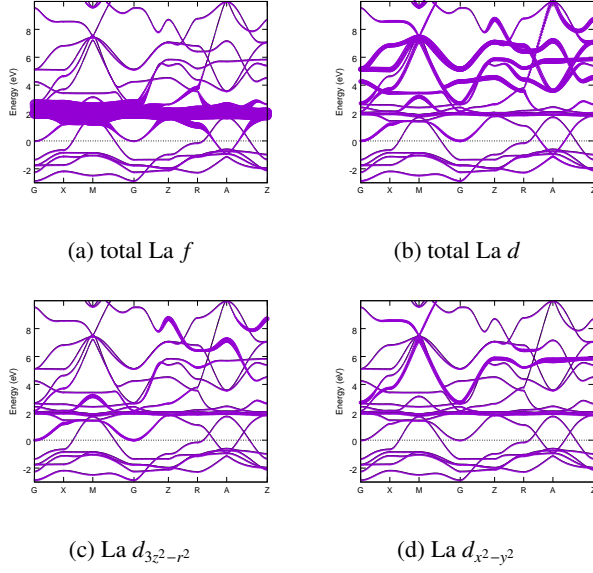


FIG. 4: Fat bands showing the amount of overlapping between Bloch states and La d states and La f states. (a) and (b): total f and total d character. (c) and (d): individual La $d_{3z^2-r^2}$ and La $d_{x^2-y^2}$ character.

II.B. Downfolding and Model Construction

The single band crossing Fermi level is dominant Ni $d_{x^2-y^2}$ -like that suggests a one-band model like that in the case of cuprate. The two-band e_g model involving both the $d_{x^2-y^2}$ -like and $d_{3z^2-r^2}$ -like bands is also motivated because of the entanglement of the two mentioned in the previous section. For a complete investigation of the relative correlation strength within the d orbital subspace, we also consider the five-band model including all d -like bands.

The downfolding technique is used to build the effective Hamiltonian in Wannier orbital basis. In the case of LaNiO_2 we have to deal with the situation of band entanglement, specifically the two e_g bands are entangled with the other three Ni d -like bands and with the La f -like bands at around +2 eV above Fermi level.

To handle such case, we employed the disentangle procedure introduced by T.Miyake and co-workers²⁸. First, a set of localized Wannier orbitals is constructed from a given correlation window (energy window around Fermi energy). It's large enough to include all or most weights of the target orbital character, so the bands of that orbital character can be well reconstructed in new Wannier orbital basis. The Wannier basis that yields the reconstructed bands (e.g. the two e_g bands in the two-band model) will act as a subset of the basis, and we can call the spanned subspace the d -space. The basis for the rest of the entire Hilbert space, which we call it r -space, are then generated by Gram-Schmidt orthogonalization. By diagonalizing the Kohn-Sham Hamiltonian in the r -space, one

gets a new set of eigen functions and eigen values. Namely, the Kohn-Sham Hamiltonian is re-diagonalized in the d -space and r -space separately, and the hybridization effect between the two subspaces is neglected.

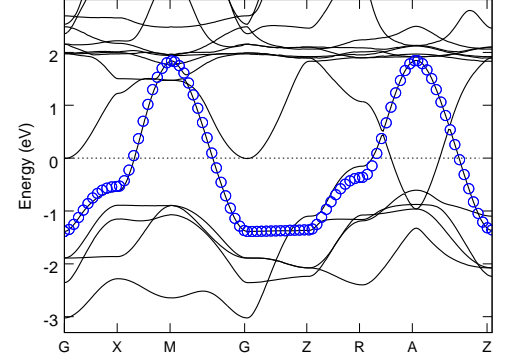


FIG. 5: Downfolded and disentangled one-band for the $d_{x^2-y^2}$ subspace. Solid lines (black) are the original Bloch bands. Circles (blue) represents the reconstructed band in Wannier orbital basis. E_F is at zero.

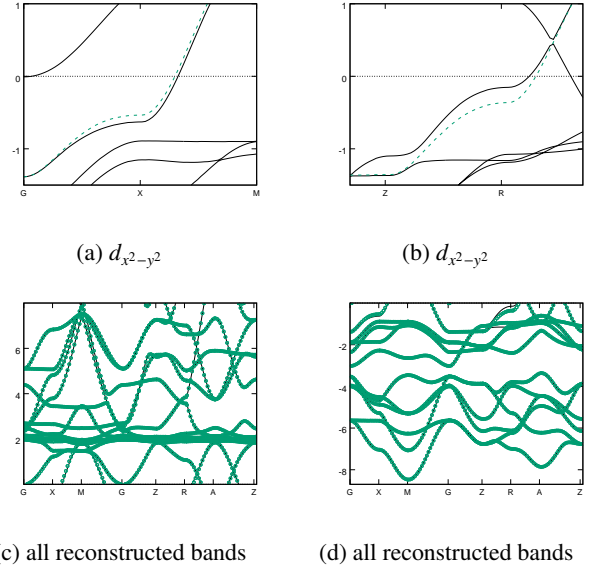


FIG. 6: Downfolded and disentangled bands for the one-band model. (a) and (b): enlarged details of the mismatching parts of the reconstructed $d_{x^2-y^2}$ band (green dash lines). (c) and (d): good matching of the reconstructed bands (green circles) in the r -space.

A good-working example of this disentangle method is the fcc structure of Ni^{28} , where it's shown there can be small mismatching of bands within the d -space but all bands in the r -space are well reconstructed and match well. The similar effect is seen in our work, as shown in Fig.5 and Fig.6 for the

one-band model. Fig.6 (a) and (b) are zooming in the details around $k=X$, Z and R of Fig.5, where small band misalignment happens in the d -space. Fig.6 (c) and (d) show the good matching of the reconstructed bands in r -space in larger energy window (good matching is obtained throughout the entire energy spectrum).

The same disentangled Wannier downfolding was done for the two-band model and the five-band model, as shown in Fig.7 and Fig.8 respectively. We noticed the misalignment around $k=X$, Z and R did not happen in this two model constructions. This is because both e_g bands are included, thus the entanglement of the two, Fig.3 (c) and (d), is not cut. The result is good matching in both d -space and r -space.

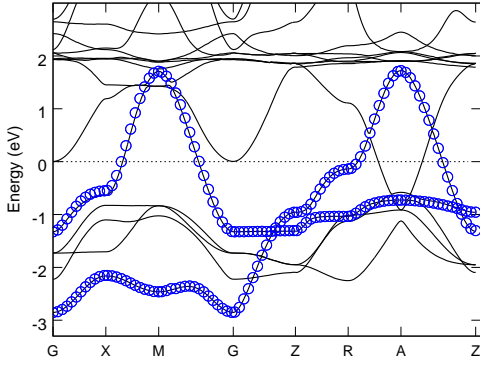


FIG. 7: Downfolded and disentangled two-band model of the $d_{x^2-y^2}$ and $d_{3z^2-r^2}$ subspace of Ni. Solid lines (black) are the original Bloch bands. Circles (blue) represents the reconstructed e_g bands in Wannier orbital basis. E_F is at zero.

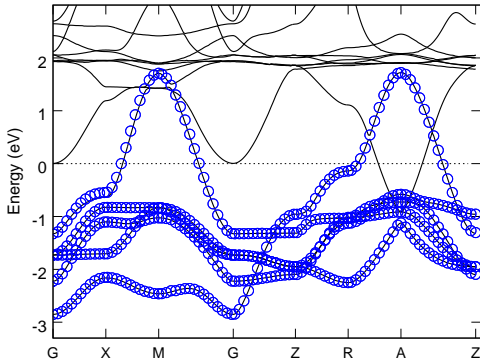


FIG. 8: Downfolded and disentangled five-band model of all d orbital subspace of Ni. Solid lines (black) are the original Bloch bands. Circles (blue) represents the reconstructed d bands in Wannier orbital basis. E_F is at zero.

II.C. cRPA calculation of U

The fully quantum description of the Coulomb interaction between two electrons occupying a multi-orbital atomic site was derived and parameterized by Kanamori²⁹. Using the language of second quantization, the Coulomb interaction term of the Hamiltonian can be written as:

$$\begin{aligned} \hat{H}_{int} = & \mathcal{U} \sum_l \hat{n}_{l\sigma} \hat{n}_{l\bar{\sigma}} \\ & + \frac{1}{2} \sum_{l \neq l'} \sum_{\sigma} [\mathcal{U}' \hat{n}_{l\sigma} \hat{n}_{l'\bar{\sigma}} + (\mathcal{U}' - \mathcal{J}) \hat{n}_{l\sigma} \hat{n}_{l'\sigma}] \\ & + \frac{1}{2} \sum_{l \neq l'} \sum_{\sigma} [\mathcal{J} \hat{c}_{l\sigma}^\dagger \hat{c}_{l'\bar{\sigma}}^\dagger \hat{c}_{l\bar{\sigma}} \hat{c}_{l'\sigma} + \mathcal{J}_c \hat{c}_{l\sigma}^\dagger \hat{c}_{l\bar{\sigma}}^\dagger \hat{c}_{l'\bar{\sigma}} \hat{c}_{l'\sigma}] \end{aligned} \quad (1)$$

where l and l' are angular momentum quantum numbers, σ and $\bar{\sigma}$ are spin and opposite-spin quantum numbers, $\hat{c}_{l\sigma}^\dagger$ and $\hat{c}_{l\sigma}$ are electron creation and annihilation operators for state (l, σ) , and $\hat{n}_{l\sigma} \equiv \hat{c}_{l\sigma}^\dagger \hat{c}_{l\sigma}$ is the density operator.

The first line of Eq.(1) represents two electrons occupying the same orbital (must be opposite spins due to the Pauli principle). The second line includes the situations where two electrons occupying two different orbitals, and they can be same or opposite spins. The two terms in the third line are called the spin-flip (coefficient \mathcal{J}) and pair-hopping (coefficient \mathcal{J}_c), which cannot be written as density-density interaction form and are often neglected (at least for nonmagnetic systems spin-flip and pair-hopping processes should have little influence). Thus, for most common cases, quantum description of the on-site Coulomb interaction requires the calculation of \mathcal{U} , \mathcal{U}' and \mathcal{J} , which are the quantities we calculate in the current work.

One way to calculate the Coulomb interaction U from first principles is the constrained Random Phase Approximation (cRPA), that has been well explained in the literature^{30,31}. In this section we briefly go over the original idea, followed by description of the implementation based on the density response function. The resulting U matrices from the three models are presented at the end.

The cRPA calculation is based on the RPA approximation where the constrain means excluding a group of orbitals to get a reduced polarization function. By doing that one gets an estimation of the partially screened Coulomb interaction for a selected group of bands of interest, e.g. localized d orbitals of a transition metal atom. The original RPA approximation considers the particle-hole polarization between all possible pairs of occupied state and unoccupied state. Within DFT the particle-hole polarization can be expressed as³²:

$$\begin{aligned} P(\mathbf{r}, \mathbf{r}', \omega) = & \sum_i^{occ.} \sum_j^{unocc.} [\psi_i^*(\mathbf{r}) \cdot \psi_j(\mathbf{r}') \cdot \psi_j^*(\mathbf{r}) \cdot \psi_i(\mathbf{r}')] \\ & \times \left(\frac{1}{\omega - \varepsilon_j + \varepsilon_i + i\delta} + \frac{1}{\omega + \varepsilon_j + \varepsilon_i - i\delta} \right) \end{aligned} \quad (2)$$

where ψ_i and ε_i are the eigen functions and eigen energies of the Kohn-Sham Hamiltonian. The summation over i and j is

restricted such that i is an occupied state and j is an unoccupied state.

Within DFT, the chosen correlation window contains the selected bands of interest that have a particular orbital character, e.g. the d -like bands of Ni in our case. Since the previous section we have followed the convention in the literatures where we labelled the bands of interests as the d -space and the bands outside the correlation window as the r -space. If both the occupied state and the unoccupied state are within the d -space, then the polarization contributes to $P_d(r, r'; \omega)$. All the other pairs of occupied and unoccupied states contribute to P_r . Thus, the total polarization is divided into two parts: $P = P_d + P_r$. The P_r is the quantity related to the partially screened Coulomb interaction³³:

$$W_r(\mathbf{r}, \mathbf{r}', \omega) = [1 - v \cdot P_r(\mathbf{r}, \mathbf{r}', \omega)]^{-1} \cdot v \quad (3)$$

where v is the bare Coulomb interaction.

According to the Hedin's equations and the GW approximation, the total polarization, P , screens the bare Coulomb interaction, v , to give the fully screened interaction W , namely:

$$W(\mathbf{r}, \mathbf{r}', \omega) = [1 - v \cdot P(\mathbf{r}, \mathbf{r}', \omega)]^{-1} \cdot v \quad (4)$$

Eq.(3) follows similar interpretation as Eq.(4) where P_r screens the bare Coulomb interaction to give the partially screened interaction W_r . At last the $U(\omega)$ matrices is calculated from the screened Coulomb interaction W_r ³⁴:

$$U_{nn'}^{TT'}(\omega) \equiv \iint |w_n^T(\mathbf{r})|^2 W_r(\mathbf{r}, \mathbf{r}', \omega) |w_{n'}^{T'}(\mathbf{r}')|^2 d\mathbf{r} d\mathbf{r}' \quad (5)$$

where $w_n(\mathbf{r})$ is the n th Wannier orbital within the d -space. The subscript n has same feature as the angular momentum quantum number l in Eq.(1). The superscript T and T' are real space lattice vectors, indicating the location of the Wannier center in real space lattice.

The key quantity in realization of the above described cRPA is to calculate the polarization function P , which is the density response function χ . In general the Kohn-Sham density response function χ^{KS} is related to the general response function χ through the following integral equation³²:

$$\chi(\mathbf{r}, \mathbf{r}', \omega) = \chi^{KS}(\mathbf{r}, \mathbf{r}', \omega) + \iint d\mathbf{r}_1 d\mathbf{r}_2 [\chi^{KS}(\mathbf{r}, \mathbf{r}_1; \omega) \cdot \left(\frac{1}{|\mathbf{r}_1 - \mathbf{r}_2|} + f^{xc}(\mathbf{r}_1, \mathbf{r}_2; \omega) \right) \cdot \chi(\mathbf{r}_2, \mathbf{r}'; \omega)] \quad (6)$$

where the Kohn-Sham response function can be written as^{32,34}:

$$\chi^{KS}(\mathbf{r}, \mathbf{r}'; \omega) = \sum_{i,j} \frac{(f_i - f_j) \psi_i^*(\mathbf{r}) \psi_j(\mathbf{r}') \psi_j^*(\mathbf{r}) \psi_i(\mathbf{r}')}{\omega - \varepsilon_j + \varepsilon_i + i\delta} \quad (7)$$

where f_i and ε_i are the occupancy and eigen energy of the eigen state ψ_i , and f^{xc} is the functional derivative of the exchange-correlation potential with respect to the charge density which is neglected in the random phase approximation³² if we assume non-interacting electrons.

The constrain (excluding the contribution from d -space) is directly applied to χ^{KS} to get χ_r^{KS} . Then χ_r is solved from the *reduced* version of Eq.(6):

$$\chi_r(\mathbf{r}, \mathbf{r}', \omega) = \chi_r^{KS}(\mathbf{r}, \mathbf{r}', \omega) + \iint d\mathbf{r}_1 d\mathbf{r}_2 [\chi_r^{KS}(\mathbf{r}, \mathbf{r}_1; \omega) \cdot \left(\frac{1}{|\mathbf{r}_1 - \mathbf{r}_2|} + f^{xc}(\mathbf{r}_1, \mathbf{r}_2; \omega) \right) \cdot \chi_r(\mathbf{r}_2, \mathbf{r}'; \omega)] \quad (8)$$

The rest steps is based on the linear response theory³⁵, where the partially screened Coulomb interaction W_r is related to inverse dielectric function ε^{-1} and bare Coulomb interaction v and ε^{-1} can be obtained from χ_r :

$$\begin{aligned} W_r(\mathbf{r}_1, \mathbf{r}_2, \omega) &= \int d\mathbf{r} [\varepsilon^{-1}(\mathbf{r}_1, \mathbf{r}, \omega) \cdot v(\mathbf{r}, \mathbf{r}_2)] \\ &= \int d\mathbf{r} [(1 + v \cdot \chi_r(\mathbf{r}_1, \mathbf{r}, \omega)) \cdot v(\mathbf{r}, \mathbf{r}_2)] \end{aligned} \quad (9)$$

At last one uses Eq.(5) to get $U_{nn'}^{TT'}(\omega)$.

The above described calculations have been implemented in the Exciting-Plus code (a modified version of ELK code)^{34,36}. In practise, 100 empty bands are included in the ground state calculation. We have benchmarked the method using late transition monoxides NiO, CoO, FeO and MnO and got results in agreement with other implementations of essentially the same method³⁷. The one, two and five Ni d bands are excluded in calculating the χ_r^{KS} , for the three models respectively. The resulting U matrices are within the Kanamori parameterization described at the beginning of this section and the parameters \mathcal{U} , \mathcal{U}' and \mathcal{J} are often organized as a U matrix and a J matrix, respectively, for example for the two-band model of $d_{3z^2-r^2}$ and $d_{x^2-y^2}$ subspace:

$$\begin{pmatrix} d_{3z^2-r^2} & d_{x^2-y^2} \\ \mathcal{U} & \mathcal{U}' \\ \mathcal{U}' & \mathcal{U} \end{pmatrix} \begin{matrix} d_{3z^2-r^2} \\ d_{x^2-y^2} \end{matrix} \quad \begin{pmatrix} d_{3z^2-r^2} & d_{x^2-y^2} \\ \mathcal{J} & \mathcal{U} \end{pmatrix} \begin{matrix} d_{3z^2-r^2} \\ d_{x^2-y^2} \end{matrix}$$

An important feature of the cRPA calculation is that it actually does not restrict to only on-site interaction because the key quantity W_r is not a local function, though most usages of the method focus on on-site interaction only, i.e. $T = T'$ in Eq.(5). If the Wannier orbital centers are chosen to be on the neighbor sites, e.g. $T - T' = N_1 \cdot \mathbf{R}_1 + N_2 \cdot \mathbf{R}_2 + N_3 \cdot \mathbf{R}_3$ with $\mathbf{R}_1, \mathbf{R}_2, \mathbf{R}_3$ being the three lattice vectors of the primitive cell and N_1, N_2, N_3 being integers, then the physical meaning of the calculated $U(\omega)$ would be the Coulomb interaction when two electrons occupy two neighbor Ni sites. The interaction strength would be of course smaller than the on-site value, but quantitative values of $U^{n,n}(\omega)$ and $U^{n,n,n}(\omega)$ are important parameters and are desirable especially when studying non-local correlations.

III. ON-SITE AND NEAREST NEIGHBOR U

We have calculated the following Coulomb interaction matrices as labelled in Fig.1: the in Ni-O plane interactions

$U^{o.s.}(\omega)$, $U^{n.n.}(\omega)$, $U^{n.n.n.}(\omega)$ and the inter Ni-O plane interaction $U_{\perp}^{n.n.}(\omega)$, where *o.s.* stands for on-site, *n.n.* stands for nearest neighbor, and *n.n.n.* stands for next nearest neighbor. From the one-band ($d_{x^2-y^2}$) model:

$$U^{o.s.}(\omega = 0) = J^{o.s.}(\omega = 0) = (\mathcal{U}) = (3.32)$$

$$U^{n.n.}(\omega = 0) = J^{n.n.}(\omega = 0) = (\mathcal{U}) = (0.50)$$

$$U_{\perp}^{n.n.}(\omega = 0) = J_{\perp}^{n.n.}(\omega = 0) = (\mathcal{U}) = (0.44)$$

$$U^{n.n.n.}(\omega = 0) = J^{n.n.n.}(\omega = 0) = (\mathcal{U}) = (0.24)$$

All the above values are in unit of eV. The on-site interaction is 3.32 eV for two electrons sitting on the single $d_{x^2-y^2}$ orbital, while the non-on-site values correspond to the situations where one electron is in one $d_{x^2-y^2}$ orbital and another electron is in a different site $d_{x^2-y^2}$ orbital. The frequency dependency of the above listed quantities are plot in Fig.(9). The ratio of $U^{o.s.}/U^{n.n.}$ increase from 6.6 at $\omega = 0$ to about 4 as ω increases to $\omega > 40$. Both $U^{n.n.}$ and $U_{\perp}^{n.n.}$ become almost ω -independent and have identical value of about 5 eV when $\omega > 40$, that suggests the inter Ni-O layer interaction $U_{\perp}^{n.n.}$ in on equal footing with the $U^{n.n.}$ within Ni-O plane.

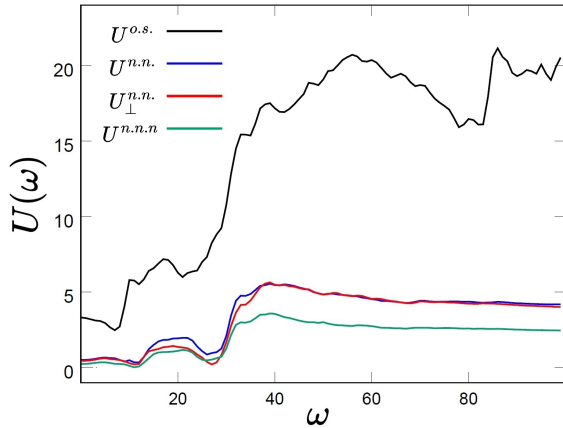


FIG. 9: Frequency dependent U of the one-band model. $U(\omega)$ is in unit of eV.

For the two-band ($d_{3z^2-r^2}$ and $d_{x^2-y^2}$) model, we got the following U and J matrices at $\omega = 0$:

$$U^{o.s.} = \begin{pmatrix} 2.86 & 1.79 \\ 1.79 & 3.27 \end{pmatrix}; \quad J^{o.s.} = \begin{pmatrix} 2.86 & 0.56 \\ 0.56 & 3.27 \end{pmatrix};$$

$$U^{n.n.} = \begin{pmatrix} 0.36 & 0.41 \\ 0.41 & 0.48 \end{pmatrix}; \quad J^{n.n.} = \begin{pmatrix} 0.36 & 0.01 \\ 0.01 & 0.48 \end{pmatrix};$$

$$U_{\perp}^{n.n.} = \begin{pmatrix} 0.63 & 0.49 \\ 0.49 & 0.41 \end{pmatrix}; \quad J_{\perp}^{n.n.} = \begin{pmatrix} 0.63 & 0.00 \\ 0.00 & 0.41 \end{pmatrix};$$

$$U^{n.n.n.} = \begin{pmatrix} 0.22 & 0.22 \\ 0.22 & 0.22 \end{pmatrix}; \quad J^{n.n.n.} = \begin{pmatrix} 0.22 & 0.00 \\ 0.00 & 0.22 \end{pmatrix};$$

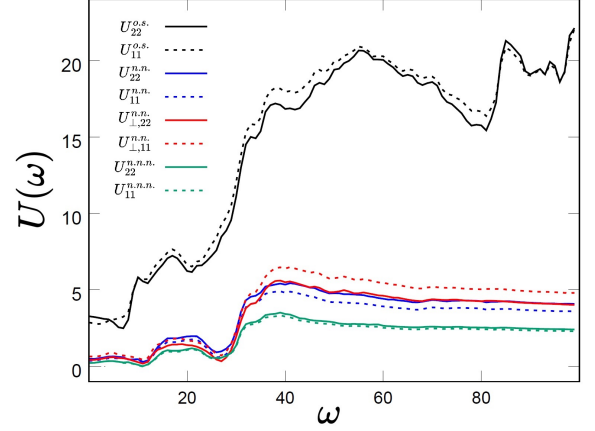


FIG. 10: Frequency dependency of the diagonal element of the U matrix of the two-band model. Unit is eV.

It's clear to see from Fig.(10) the two diagonal elements of on-site interaction (black solid and black dash curves) have almost identical frequency dependency over the whole range, though they differ by about 0.4 eV at $\omega = 0$. It suggests the Coulomb interaction strength is same no matter two electrons both on the $d_{x^2-y^2}$ orbital or both on the $d_{3z^2-r^2}$ orbital. And the observation is in consistency with that from the one-band model. Another observation that's same as the one-band model is the almost identical in-plane and inter-plane nearest neighbor interactions, $U_{22}^{n.n.}$ and $U_{\perp,22}^{n.n.}$ for the $d_{x^2-y^2}$ orbital (blue and red solid lines). However the $U_{11}^{n.n.}$ and $U_{\perp,11}^{n.n.}$ for the $d_{3z^2-r^2}$ orbital (blue and red dash lines) are different, where the inter Ni-O plane interaction is greater. When $\omega > 40$ the difference keeps at about 1.25 eV steady. An additional results from the two-band model is the off-diagonal elements of $J^{n.n.}$ and $J_{\perp}^{n.n.}$ being zero, i.e. the parameter \mathcal{J} is zero. Recall the two density-density terms in the second line of Eq.(1) and the picture where one electron sits in the $d_{x^2-y^2}$ (or $d_{3z^2-r^2}$) orbital and another electron sits in the other orbital of a nearest neighbor site, $\mathcal{J} = 0$ means the interaction strength does not care whether the two spins are parallel or anti-parallel. And, the same for $J^{n.n.n.}$.

At last, $U^{n.n.n.}$ is of same features in the two models. The two-band model does not present any new feature for the $d_{3z^2-r^2}$ orbital, it's same as the $d_{x^2-y^2}$ orbital.

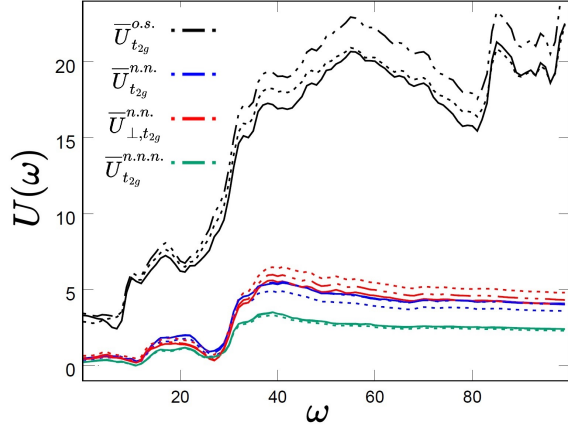


FIG. 11: Frequency dependency of the diagonal element of the U matrix of the five-band model. Unit is eV.

IV. SUMMARY AND CONCLUSION

In summary, we performed DFT calculation of bulk LaNiO_2 in its non-magnetic phase, and constructed different model Hamiltonians including the single $d_{x^2-y^2}$ orbital, the e_g orbitals and all five d orbitals of Ni. And we performed cRPA calculations of the Coulomb interactions for the on-site d orbitals and Coulomb interactions for the d orbitals between neighbor sites, for the constructed models. The resulting Coulomb interaction parameters of the $d_{x^2-y^2}$ orbital are consistent within all three models. The results for the e_g orbitals from the two-band model agree with that from the five-band model too.

The ratio of $U^{o.s.}(\omega)/U^{n.n.}(\omega)$ is found to be 6.6 at $\omega = 0$ and drops to about 4 when $\omega > 40$, indicating a pretty strong non-local Coulomb interaction. The inter Ni-O plane nearest neighbor Coulomb interaction is found to be almost exactly same as the in plane one, $U^{n.n.}(\omega)/U^{\perp, n.n.}(\omega) \approx 1$. It suggest the material is non-locally correlated in all x, y and z directions. In the longer range, we found $U^{n.n.n.}$ is about 50%-60% of the $U^{n.n.}$ over the entire frequency range.

In conclusion, the presented work provides a quantitative and detailed description of the local and non-local Coulomb interaction strengths of the Ni d -orbitals in LaNiO_2 from first principle. The numerical study suggests a not very strong but very non-local electron correlation of this material, that could benefit future DFT calculations as well as model calculations of the nickelate family of superconductors.

- ¹ J. G. Bednorz and K. A. Muller, *Zeitschrift fur Physik B Condensed Matter* **64**, 189 (1986).
- ² B. Keimer, S. A. Kivelson, M. R. Norman, S. Uchida, and J. Zaanen, *Nature* **518**, 179 (2015).
- ³ P. A. Lee, N. Nagaosa, and X.-G. Wen, *Rev. Mod. Phys.* **78**, 17 (2006).
- ⁴ D. J. Scalapino, *Rev. Mod. Phys.* **84**, 1383 (2012).
- ⁵ C. C. Tsuei and J. R. Kirtley, *Rev. Mod. Phys.* **72**, 969 (2000).
- ⁶ A. Damascelli, Z. Hussain, and Z.-X. Shen, *Rev. Mod. Phys.* **75**, 473 (2003).
- ⁷ M. R. Norman, *Reports on Progress in Physics* **79**, 074502 (2016).
- ⁸ J. Zhang, A. S. Botana, J. W. Freeland, D. Phelan, H. Zhang, V. Pardo, M. R. Norman, and J. F. Michell, *Nature Physics* **13**, 864 (2017).
- ⁹ A. V. Boris, Y. Matiks, E. Benckiser, A. Frano, P. Popovich, V. Hinkov, P. Wochner, M. Castro-Colin, E. Detemple, V. K. Malik, C. Bernhard, T. Prokscha, A. Suter, Z. Salman, E. Morenzoni, G. Cristiani, H.-U. Habermeier, and B. Keimer, *Science* **332**, 937 (2011), <https://www.science.org/doi/pdf/10.1126/science.1202647>.
- ¹⁰ M. J. Han, X. Wang, C. A. Marianetti, and A. J. Millis, *Phys. Rev. Lett.* **107**, 206804 (2011).
- ¹¹ P. Hansmann, X. Yang, A. Toschi, G. Khaliullin, O. K. Andersen, and K. Held, *Phys. Rev. Lett.* **103**, 016401 (2009).
- ¹² M. Uchida, K. Ishizaka, P. Hansmann, Y. Kaneko, Y. Ishida, X. Yang, R. Kumai, A. Toschi, Y. Onose, R. Arita, K. Held, O. K. Andersen, S. Shin, and Y. Tokura, *Phys. Rev. Lett.* **106**, 027001 (2011).
- ¹³ J. c. v. Chaloupka and G. Khaliullin, *Phys. Rev. Lett.* **100**, 016404 (2008).
- ¹⁴ D. Li, K. Lee, B. Y. Wang, M. Osada, S. Crossley, H. R. Lee, Y. Cui, Y. Hikita, and H. Y. Hwang, *Nature* **572**, 624 (2019).
- ¹⁵ D. Li, B. Y. Wang, K. Lee, S. P. Harvey, M. Osada, B. H. Goodge, L. F. Kourkoutis, and H. Y. Hwang, *Phys. Rev. Lett.* **125**, 027001 (2020).
- ¹⁶ S. Zeng, C. S. Tang, X. Yin, C. Li, M. Li, Z. Huang, J. Hu, W. Liu, G. J. Omar, H. Jani, Z. S. Lim, K. Han, D. Wan, P. Yang, S. J. Pennycook, A. T. S. Wee, and A. Ariando, *Phys. Rev. Lett.* **125**, 147003 (2020).
- ¹⁷ M. Hayward and M. Rosseinsky, *Solid State Sciences* **5**, 839 (2003), international Conference on Inorganic Materials 2002.
- ¹⁸ M. Cresspin, P. Levitz, and L. Gatineau, *J. Chem. Soc., Faraday Trans. 2* **79**, 1181 (1983).
- ¹⁹ K.-W. Lee and W. E. Pickett, *Phys. Rev. B* **70**, 165109 (2004).
- ²⁰ R. Zhang, C. Lane, B. Singh, J. Nokelainen, B. Barbiellini, R. S. Markiewicz, A. Bansil, and J. Sun, *Communications Physics* **4**, 2399 (2021).
- ²¹ B.-X. Wang, H. Zheng, E. Krivyakina, O. Chmaissem, P. P. Lopes, J. W. Lynn, L. C. Gallington, Y. Ren, S. Rosenkranz, J. F. Mitchell, and D. Phelan, *Phys. Rev. Materials* **4**, 084409 (2020).
- ²² M. A. Hayward, M. A. Green, M. J. Rosseinsky, and J. Sloan, *Journal of the American Chemical Society* **121**, 8843 (1999), <https://doi.org/10.1021/ja991573i>.
- ²³ A. S. Botana and M. R. Norman, *Phys. Rev. X* **10**, 011024 (2020).
- ²⁴ H. Watanabe, T. Shirakawa, K. Seki, H. Sakakibara, T. Kotani, H. Ikeda, and S. Yunoki, *Phys. Rev. Research* **3**, 033157 (2021).
- ²⁵ H. Sakakibara, H. Usui, K. Suzuki, T. Kotani, H. Aoki, and K. Kuroki, *Phys. Rev. Lett.* **125**, 077003 (2020).
- ²⁶ Y. Wang, C.-J. Kang, H. Miao, and G. Kotliar, *Phys. Rev. B* **102**, 161118 (2020).
- ²⁷ A. Kozhevnikov, A. G. Eguiluz, and T. C. Schulthess, 2010 ACM/IEEE International Conference for High Performance Computing, Networking, Storage and Analysis, 1 (2010).
- ²⁸ T. Miyake, F. Aryasetiawan, and M. Imada, *Phys. Rev. B* **80**, 155134 (2009).
- ²⁹ J. Kanamori, *Progress of Theoretical Physics* **30**, 275 (1963).
- ³⁰ F. Aryasetiawan, M. Imada, A. Georges, G. Kotliar, S. Biermann, and A. I. Lichtenstein, *Phys. Rev. B* **70**, 195104 (2004).
- ³¹ F. Aryasetiawan, K. Karlsson, O. Jepsen, and U. Schönberger, *Phys. Rev. B* **74**, 125106 (2006).
- ³² M. Petersilka, U. J. Gossmann, and E. K. U. Gross, *Phys. Rev. Lett.* **76**, 1212 (1996).
- ³³ F. Aryasetiawan, M. Imada, A. Georges, G. Kotliar, S. Biermann, and A. I. Lichtenstein, *Phys. Rev. B* **70**, 195104 (2004).
- ³⁴ A. Kozhevnikov, A. G. Eguiluz, and T. C. Schulthess, in *SC '10: Proceedings of the 2010 ACM/IEEE International Conference for High Performance Computing, Networking, Storage and Analysis* (2010) pp. 1–10.
- ³⁵ A. A. Dyachenko, A. O. Shorikov, A. V. Lukoyanov, and V. I. Anisimov, *JETP Letters* **96**, 56 (2012).
- ³⁶ “ELK: an all-electron full-potential linearised augmented-plane wave code,” <http://elk.sourceforge.net/> (2018).
- ³⁷ L. Zhang, P. Staar, A. Kozhevnikov, Y.-P. Wang, J. Trinastic, T. Schulthess, and H.-P. Cheng, *Phys. Rev. B* **100**, 035104 (2019).